International Journal of Engineering, Mathematical and Physical Sciences
ISSN: 2517-9934
Vol:11, No:10, 2017

Investigating the Effects of Thermal and Surface Energy on the Two-Dimensional Flow Characteristics of Oil in Water Mixture between Two Parallel Plates: A Lattice Boltzmann Method Study

W. Hasan, H. Farhat

***Abstract*—**A hybrid quasi-steady thermal lattice Boltzmann model was used to study the combined effects of temperature and contact angle on the movement of slugs and droplets of oil in water (O/W) system flowing between two parallel plates. The model static contact angle due to the deposition of the O/W droplet on a flat surface with simulated hydrophilic characteristic at different fluid temperatures, matched very well the proposed theoretical calculation. Furthermore, the model was used to simulate the dynamic behavior of droplets and slugs deposited on the domain's upper and lower surfaces, while subjected to parabolic flow conditions. The model accurately simulated the contact angle hysteresis for the dynamic droplets cases. It was also shown that at elevated temperatures the required power to transport the mixture diminished remarkably.

***Keywords*—**Lattice Boltzmann method, Gunstensen model, thermal, contact angle, high viscosity ratio.

I. Introduction

CRUDE oil recovery is an important process, in which oil extraction has many difficulties in the miscellaneous stages of production and development. Thermal recovery method is used to improve the crude oil mobility especially for reservoirs containing heavy oil [1].

Babadagli and Al-Bemani [2] studied the influence of steam injection on heavy oil inside carbonate reservoir rock. They found that the mechanism of thermal expansion was the main cause of the recovery.

Babadagli [3] investigated the role of temperature on the mechanism of capillary imbibition. He used 3D capillary imbibition tests with a temperature range of 20-90°C. Babadagli utilized different types of O/W with wide range of interfacial tensions and viscosity ratios. The author found a reduction in interfacial tension and viscosity as temperature increased, which significantly altered the rate of capillary imbibition.

Several research efforts targeted the chalk-water-crude oil interactions [4]-[10]. The authors showed that in the oil-water- rock system, the increase in temperature led to improving the water wetness of oil-wet chalk and resulted in an increased oil recovery, associated with a considerable reduction in interfacial tension and contact angle.

Al-Hadhrami and Blunt [11], [12] investigated the effect of temperature on the wettability alteration in oil-wet fractured carbonate reservoirs. They used hot-water injection and steam flooding in their investigation. Their results showed that as temperature increased the wettability changed from oil-wet to water-wet.

Briggs et al. [13] studied heavy oil field numerically. They concluded that the oil viscosity had to be reduced in order to increase the efficiency of capillary imbibition, which led to an increased oil recovery. This target was accomplished by introducing heat into the oil field.

Shi and Dhir [14] used Lennard-Jones molecular dynamics approach for simulating liquid and water droplets adjacent to a solid surface. The contact angle was obtained by using direct simulation. The particle-particle, particle-mesh method for long-range force correction was used in the simulation. The contact angle was derived as a function of system temperature and the solid/fluid interaction potential. The study concluded that the contact angle decreased with increasing system temperature and increased when the potential decreased.

Huang et al. [15] proposed a method for approximating the adhesion parameters in the Shan and Chen multicomponent, multiphase lattice Boltzmann model, which leads to the desired fluid-solid contact angle. The method is a straightforward application of Young's equation with substitution of the Shan and Chen cohesion parameter with a density factor for the fluid-fluid interfacial tension, and the adhesion parameters for the corresponding fluid-solid interfacial tensions.

In this work, a thermal lattice Boltzmann model is coupled with a temperature dependent interfacial tension and contact angle modules to study the combined multi-physics effects on SAE-50 O/W system. The thermal-capillary effects have direct impact on the transport properties of crude oil. The model static contact angles on two channels with different surface energies were validated at different temperatures by comparison with the results of the mathematical model. The model was also used to simulate the dynamic behavior of the O/W system flowing between two parallel plates. Oil slugs and droplets attached to the upper and lower walls were investigated. The aim is to improve our understanding of the underlying physics associated with the secondary and tertiary extraction process of trapped crude oil in wells by injecting

W. Hasan is with the North Oil Company, Kirkuk, Iraq, Department of Mechanical Engineering, Wayne State University, Detroit, MI, USA.

H. Farhat is with the Department of Mechanical Engineering, Wayne State University, Detroit, MI, USA (corresponding author, e-mail: av9328@wayne.edu).

hot water.

II. Numerical Method

A. LBM and the Gunstensen Model

The Bhatnagar-Gross-Krook (BGK) lattice Boltzmann (LBM) isothermal, single-relaxation model used in this work. LBM basic equation is derived from the Boltzmann kinetic equation:

$$\frac{df}{dt}+\boldsymbol{\xi}\cdot\nabla f=-\frac{1}{\lambda}(f-f^{eq}) \tag{1}$$

where f is the density distribution function, $\boldsymbol{\xi}$ is the macroscopic velocity, f^{eq} is the equilibrium distribution function, and λ is the physical relaxation time. Equation (1) is first discretized by using a set of velocities $\{\xi_i\}$ confined to a finite number of directions and this leads to:

$$\frac{df_i}{dt}+\boldsymbol{\xi}_i\cdot\nabla f_i=-\frac{1}{\lambda}(f_i-f_i^{eq}) \tag{2}$$

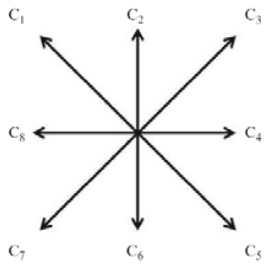

Fig. 1 Velocity vectors for the D2Q9 lattice Boltzmann method used in this model

The Gunstensen multi-component model uses a color blind total density distribution function given by:

$$f_i(\boldsymbol{x},t)=f_i^{L}(\boldsymbol{x},t)+f_i^{H}(\boldsymbol{x},t) \tag{3}$$

The collision step is first executed by using:

$$\begin{aligned}\hat{f}_i^{q}(x,t+\delta_t)&=f_i^{q}(x,t)-\frac{1}{\tau^{q}}\times\\ &[f_i^{q}(x,t)-f_i^{q,eq}(\rho,\rho u)]+\phi_i(x)\end{aligned} \tag{4}$$

The lattice space δ_x and the lattice time step δ_t are taken as unity and their ratio $c=\delta_x/\delta_t=1$, while q refers to the light and heavy fluids and $\phi_i(x)$ is the source term.

A phase field function is used to track the O/W interface and it is calculated as:

$$\rho^{N}(\boldsymbol{x},t)=\frac{\rho^{L}(\boldsymbol{x},t)-\rho^{H}(\boldsymbol{x},t)}{\rho^{L}(\boldsymbol{x},t)+\rho^{H}(\boldsymbol{x},t)} \tag{5}$$

The constituent fluids densities are given by:

$$\begin{aligned}\rho^{L}(\boldsymbol{x},t)&=\sum_{0}^{Q-1}f_i^{L}(\boldsymbol{x},t)\\ \rho^{H}(\boldsymbol{x},t)&=\sum_{0}^{Q-1}f_i^{H}(\boldsymbol{x},t)\end{aligned} \tag{6}$$

After collision, the mixture is segregated, and the streaming step is executed by:

$$\begin{aligned}f_i^{L}(\boldsymbol{x}+\boldsymbol{c}_i\delta_t,t+\delta_t)&=\hat{\hat{f}}_i^{L}(\boldsymbol{x},t+\delta_t)\\ f_i^{H}(\boldsymbol{x}+\boldsymbol{c}_i\delta_t,t+\delta_t)&=\hat{\hat{f}}_i^{H}(\boldsymbol{x},t+\delta_t)\end{aligned} \tag{7}$$

The macroscopic density and momentum are obtained from the distribution function as:

$$\rho=\sum_{i=0}^{Q-1}f_i=\sum_{i=0}^{Q-1}f_i^{eq} \tag{8}$$

$$\rho\boldsymbol{u}=\sum_{i=1}^{Q-1}\boldsymbol{c}_i f_i=\sum_{i=1}^{Q-1}\boldsymbol{c}_i f_i^{eq} \tag{9}$$

The kinematic viscosity is a function of the lattice relaxation time τ, the square of speed of sound c_s and it is given by:

$$\nu=(\tau-0.5)c_s^2\delta_t \tag{10}$$

B. The Quasi-Steady Thermal Model

Assuming small variations in the thermal fluid properties and no phase change due to temperature rise or fall, the following energy equation is used for the calculation of the flow temperature profile:

$$\partial_t T+\nabla\cdot(\boldsymbol{u}T)=D_{ifs}\nabla^2 T+\varphi \tag{11}$$

In (11) $\partial_t T$ accounts for the fluid temperature change in time, $\nabla\cdot(\boldsymbol{u}T)$ is the convection term, and $D_{ifs}\nabla^2 T$ is the diffusion term, φ accounts for the flow viscous dissipation. It is important to note that in the described model the lattice physical temperatures have a one to one relation. For more information about the thermal model the reader is referred to Hasan et al. [16].

C. The Surface Tension Temperature Depended Model

The temperature dependent surface tension used here was presented in the work of Ganesan et al. [17].

$$\sigma(T_f)=\sigma_{ref}-C_1(T_f-T_{ref}) \tag{12}$$

The value for C_1 was calculated by using physical data for

oil in water system shown in Table I.

TABLE I
INTERFACIAL TENSIONS AT DIFFERENT TEMPERATURES

Temperature (°C)	Interfacial Tension (N/m)
0	0.0271
10	0.0253
20	0.0235
30	0.0217
40	0.0199
50	0.0181
60	0.0163
70	0.0145
80	0.0127

In order to use (10) for the simulation, the lattice initial surface tension σ_0 was selected such that the lattice Eötvös number matched the physical number given by:

$$Eo = \frac{\Delta\rho g \ell^2}{\sigma_0} \tag{13}$$

where ℓ is the characteristic length and g is acceleration due to gravity of the matrix and $\Delta\rho$ is the density difference.

D. The Contact Angle Temperature Depended Model

Venkatesan et al. [18] derived the following theoretical temperature dependent contact angle equation:

$$\theta_d\left(T_F\right) = \cos^{-1}\left(\frac{\cos\theta^{ref}}{1-\frac{C_1}{\sigma_{ref}}\left(T_F-1\right)}\right) \tag{14}$$

where, θ_d is the temperature dependent dynamic contact angle, θ^{ref} is the equilibrium contact angle at the reference temperature, and σ_{ref} is the interfacial tension at reference temperature.

The contact angle in the Gunstensen LBM can be achieved by assigning a phase field value for the wall. The calculated angles from (14) for several reference temperatures and contact surfaces, were used for determining the appropriate phase field values for the targeted contact angles. These values were curve fitted using second order and exponential polynomial formulas and the fitted curves equations were eventually used in the code for simulating variety of cases.

III. SIMULATION AND DISCUSSION

A two-dimensional (2D) domain representing a flow between two plates was used in the subsequent simulations. Three configurations were executed in the following simulations. The first consisted of $71\times31\left[lu^2\right]$ domain and a central droplet radius $R=8\left[lu\right]$ deposited on the lower surface. The objective was to investigate the conformance of the temperature dependent static contact angle to the theoretical calculation results. The second configuration consisted of $140\times20\left[lu^2\right]$ to simulate the flow of one and two oil slugs attached to the top and bottom surfaces at different static temperatures. The last configuration consisted of $311\times49\left[lu^2\right]$ and droplet radius $R=15\left[lu\right]$ and it was used to simulate the movement of four droplets placed on the upper and lower surfaces with three different static temperatures. The second configuration flow was subjected to a source term $\phi_i\left(x\right)=\frac{\Delta p}{\ell}=0.000002$ and the third configuration to a source $\phi_i\left(x\right)=\frac{\Delta p}{\ell}=0.000001$. This was to induce constant pressure gradient, which when associated with a second-order bounce back on the top and bottom surfaces resulted in a disturbed parabolic flow profile. Periodic boundary condition was imposed on the inlet and outlet boundaries. Dimensionless variables were used in the analysis of the simulation results with reference time calculated as follows: $\dot{\gamma}_{1/4(h)}\times t$ where $\dot{\gamma}$ is the shear strain rate calculated at $\frac{h}{4}$ with h as the channel height and t as the time step. The height of the channel was used as the reference distance and the central velocity of the undisturbed parabolic flow was used as the reference velocity calculated by: $u_{\max}=\frac{h^2}{2\mu}\times\frac{\Delta p}{\ell}$.

The physical Eötvös number calculated at $T_{av}=40c^o$ is equal to 1.475×10^{-4}. Gravitational acceleration $g=5.46\times10^{-9}\left[lu\times ts^{-2}\right]$ and mixture interfacial tension $\sigma_0=0.01028\left[lf\times lu^{-1}\right]$ were used to insure Eötvös number similarity.

A. Validating the Temperature Dependent Static Contact Angle

The first 2D configuration subjected was used without any source term, to check the values of the dependency of the contact angles on the domains temperature. The first case was done by assuming a reference contact angle of $\theta=66.7^o$ at $T=20^oC$. Several temperatures were used and the corresponding values of the static contact angles were measured directly from the simulations. The model was set to give the required theoretical contact angle calculated by (14) through changing the value of phase field assigned to the wall nodes by (5). The measurement results were then compared with the data from the mathematical calculations. Furthermore, a second set of simulations was done by assuming a reference contact angle of $\theta=45^o$ at $T=20^0C$ and the same procedure was adopted to check the model robustness.

A trend of diminishing static contact angle is associated with the increase in temperature of the fluid for both reference angles. The results for $\theta=66.7^o$ and $\theta=45^o$ were fitted and

the following regression formulae were found to describe their behavior:

$$\theta = -0.1052Exp(0.06148T) + 68.1Exp(-0.002053T)$$
$$\theta = -0.01325T^2 + 0.2065T + 45.84$$

Tables II and III show the values of the calculated and the measured contact angles for both validation cases. The static contact angle dependency on temperature results are presented in Fig. 2. The measured contact angles from the simulations matched very well the calculated angles for the range of temperatures and for the two-different reference static contact angles.

TABLE II
VALUES OF CALCULATED, MEASURED AND RELATIVE ERRORS FOR CONTACT ANGLE FOR VALIDATION-1

Temperature (°C)	Calculated Contact Angle	Measured Contact Angle	Relative Error (%)
20	66.7	65	2.54
40	62.2	61.5	1.12
60	55.3	56	1.26
80	43.1	43.4	0.69

TABLE III
VALUES OF CALCULATED, MEASURED AND RELATIVE ERRORS FOR CONTACT ANGLE FOR VALIDATION-2

Temperature (°C)	Calculated Contact Angle	Measured Contact Angle	Relative Error (%)
20	45	44.7	0.70
30	40	40	0.11
40	33.4	33	1.21
50	23.4	23	1.67

B. Simulating the Behavior of One and Two Slugs in Parabolic Flow at Different Temperatures

The domain consisting of $140\times20\left[lu^2\right]$ was used in this simulation with attached one and two slugs to the top and bottom walls. Three different temperatures were used in the presented simulations. As shown in Fig. 3, with $T = 40^oC$, the applied source term was able to induce slug movement inside the channel. At fluid and wall temperature $T = 50^oC$, the slug moved faster and at $T = 60^oC$, the same source term was sufficient for moving the slug from its original position towards the end of the domain at higher speed. This was due to the reduced interfacial tension as a function of temperature, which allowed less energy dissipation into deforming the droplet. Furthermore, the reduced viscosity effects upon the rise in temperature, which resulted in higher average velocity of the flow, enhanced flow transport capabilities by imparting higher flow momentum on the slug. It is important to mention that the increasing adhesion force with temperature between the slug and the walls affects the flow average velocity, however this effect is marginalized by the higher flow momentum due to the diminishing viscosity with temperature while exhibiting small difference in the fluids density.

The flow average velocity profile shown in Fig. 3 indicates the presence of fluctuations resembling a short wave and the slug moves like a caterpillar. It is clear from the velocity profile that the slug movement is due to a periodic detachment of one end after another. The dip in the average velocity shown in Fig. 3 is due to that a portion of the flow energy is absorbed in the slug interface, which eventually is released back, when an additional energy buildup from the flow subjected to constant source term, overcomes the adhesion force of the slug at one of its end.

Fig. 4 represents the behavior of two slugs subjected to the same source term between two plates at different temperatures. At $T = 40^oC$ the slugs failed to move due to the high interfacial tension, which allows the slugs to dissipate a larger portion of the flow energy and transforms it into very small deformation. On the other hand, the higher viscosity of both fluids at the prescribed temperature allows the formation of a thicker boundary layer, leading to a lower average velocity of the flow, thus depriving the slugs from the required momentum to overcome its higher adhesion force on both walls. When temperature increased to $T = 50^oC$ the slugs were able to move due to the reduced interfacial tension as a function of temperature and at $T = 60^oC$ the slugs moved faster. The flow average velocity profile shown in Fig. 4 indicates the presence of the same fluctuating motion as in the previous case, with a remarkable jump in average velocity in the case of two slugs at high temperature. This could be explained by the possibility that the two slugs may have continually detached from the walls within a small time-step difference. Since the two slugs constitute a considerable mass of the whole flow, a higher local fluctuation in the average velocity can be expected.

C. Droplets Flow between Two Parallel Plates at Different Temperatures

The $311\times49\left[lu^2\right]$ domain containing four droplets with initial radius $R_i = 15$ placed on the upper and lower surfaces was used for the dynamic simulation of multi-drops the O/W system. The second configuration source term was used to induce the droplets movement between the two parallel plates at two different temperatures.

The droplets with domains and fluid's temperatures $T = 20^oC$ and $T = 40^oC$, showed movement of the droplets because of the smaller adhesion force compared to the slug case. It is obvious from Fig. 5 that the average flow velocity is almost doubled at higher temperature and that droplets transportation is more efficient for the same reasons mentioned in the previous section. The average flow velocity for all cases showed much less fluctuation. This is because the droplets are sticking to one side of the domain.

The average contact angle hysteresis for temperatures $T = 20^oC$, $T = 40^oC$ and $T = 50^oC$ was measured as $\Delta\theta = 7.3$, $\Delta\theta = 8.5$ and $\Delta\theta = 10.8$, respectively. The higher contact hysteresis associated with the higher temperature is due to lower droplets' interfacial tension and higher adhesion force.

The streamlines in Fig. 5 show the droplets at lower temperature, and hence the higher viscosity and interfacial tension act like a physical obstacle toward the suspending flow movement.

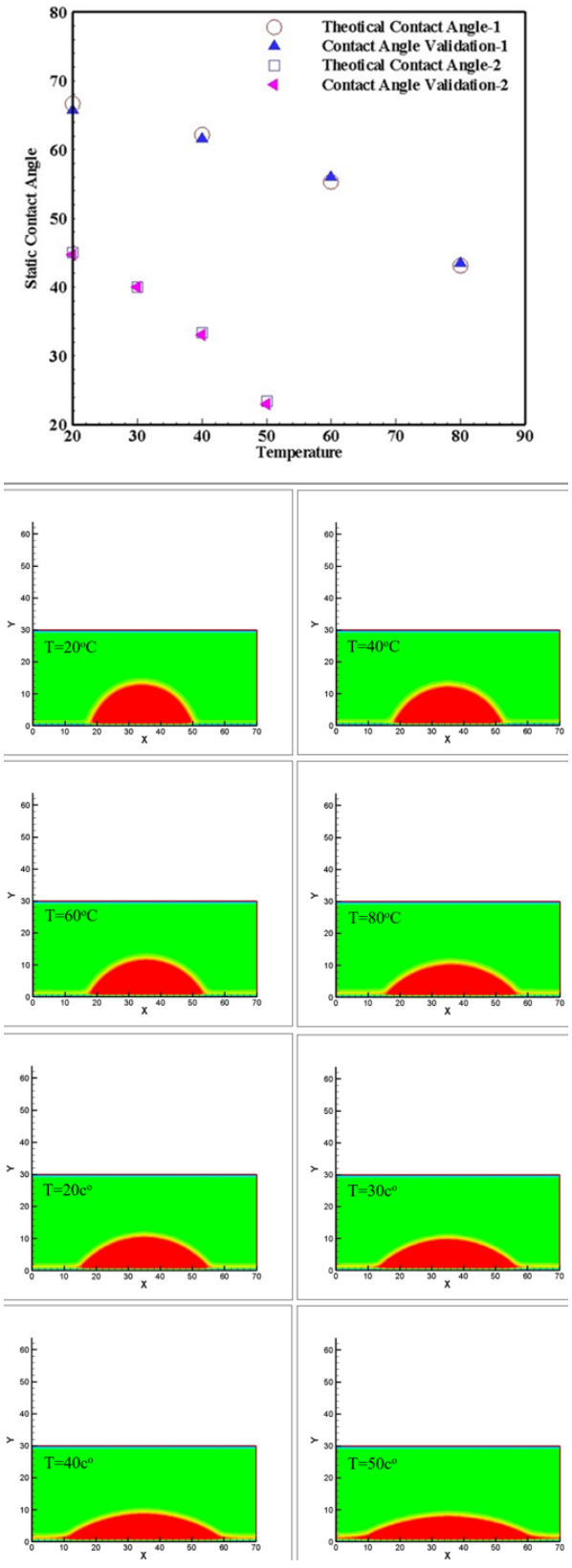

Fig. 2 Static contact angles at different temperatures for the first and the second validation cases and static contact angle vs. temperature

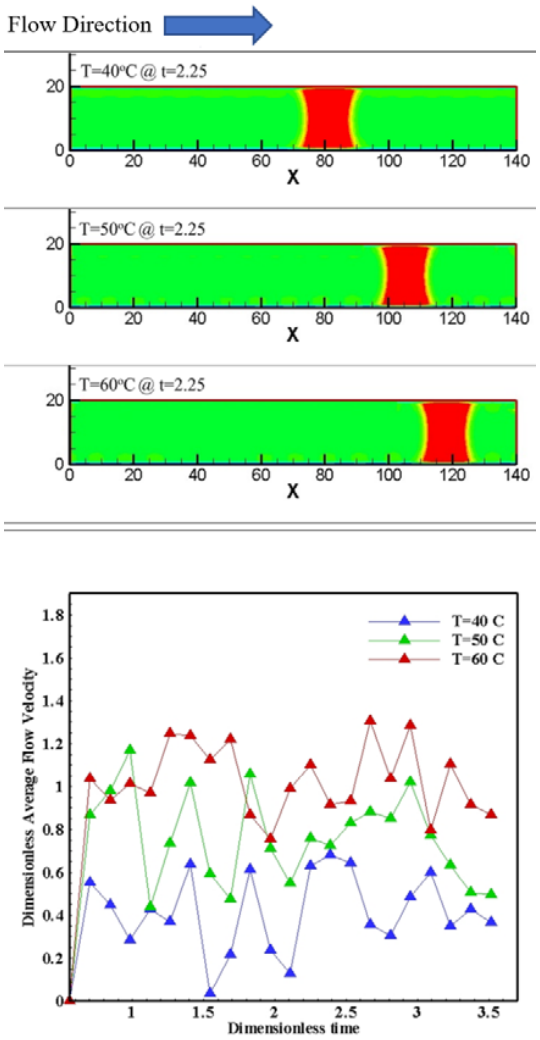

Fig. 3 One slug displacement at different temperatures and same dimensionless time

D. Flow Power Number Ratio

The power content in the undisturbed flow through the channel is calculated by [19]:

$$Q = \int_{-h}^{h} u dy = \frac{2h^3 \Delta p}{3\mu \ell} = 2u_{ave} h \tag{15}$$

where Q is the volumetric flow rate through the channel, $F = \Delta p / \ell$ is the applied source term, u_{ave} is the average undistributed flow velocity and h is half channel height.

The power required for moving the undisturbed flow through the channel is calculated by:

$$\mathrm{P} = Q\, \Delta p = \frac{2h^3 F^2 \ell}{3\mu} = 2u_{ave} h F \ell \tag{16}$$

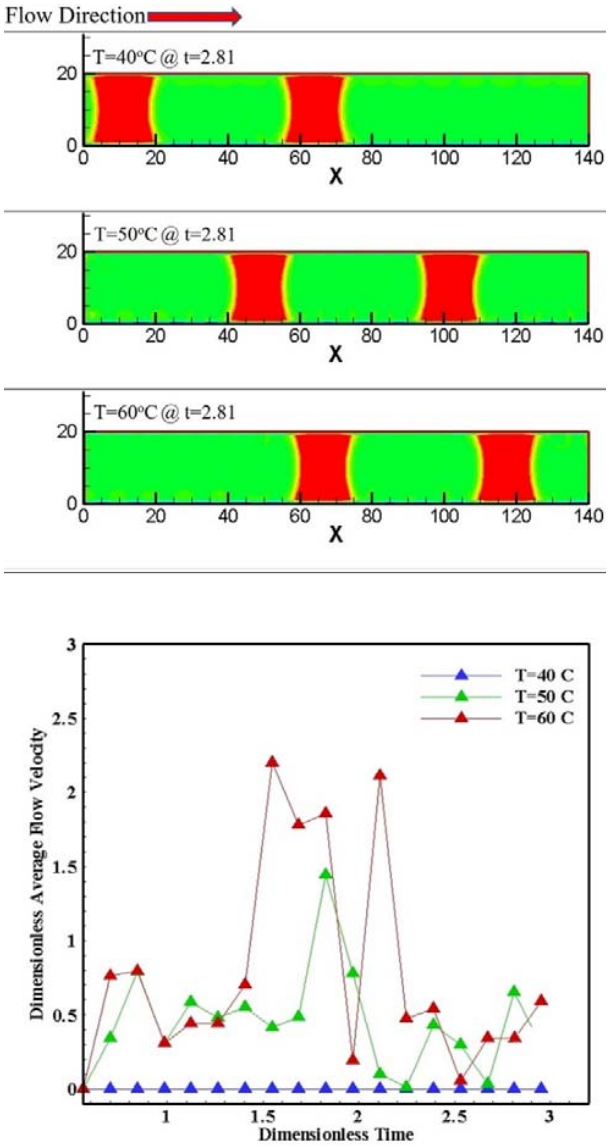

Fig. 4 Two slugs' displacement at different temperatures and same dimensionless time

The combined droplets' mass center displacement was tracked in the simulations at equally spaced time steps. The suspended phase velocity was then calculated by numerically differentiating the mass center displacement using second order accuracy finite difference scheme. A droplet power number was derived as follows:

$$P_d = \frac{\rho_d \forall_d V_{dmc}^3}{\ell} \quad (17)$$

Here ρ_d is the droplet density, $\forall_d$ is the initial combined droplets' volume, V_{dmc} is the combined droplets' mass center terminal velocity and ℓ is the domain length.

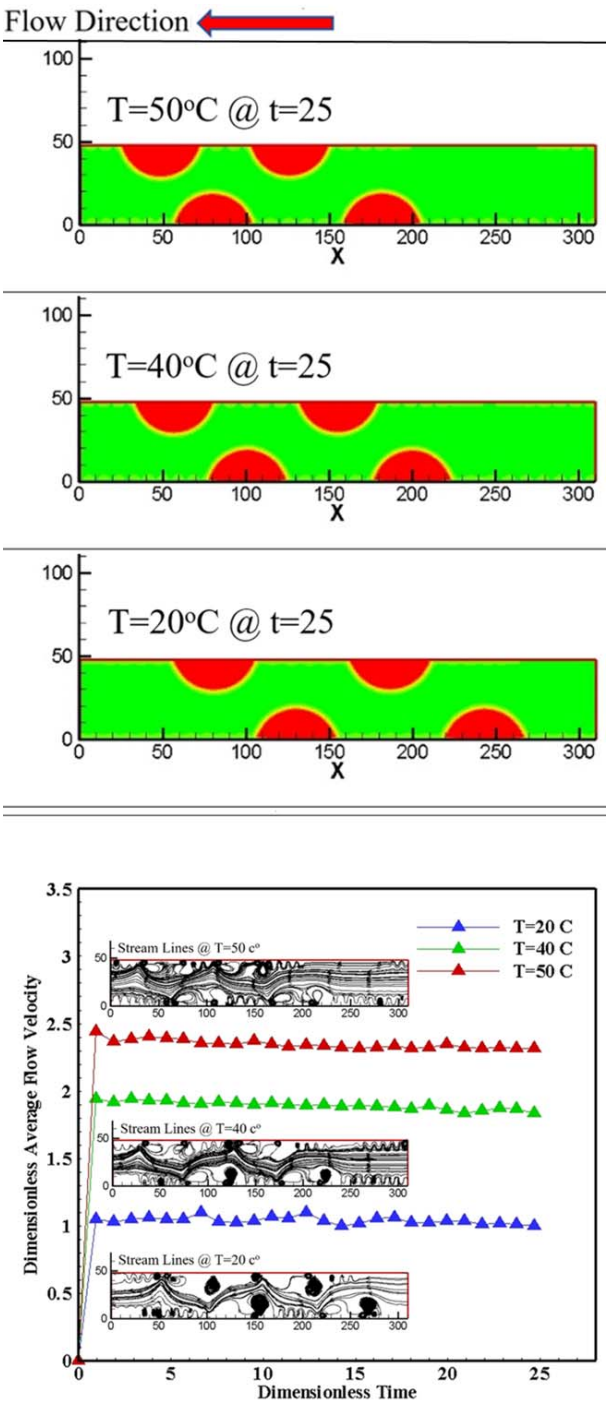

Fig. 5 Droplets displacement at two different temperatures and same times with negative source term. Insets are for the streamlines of the various cases

The power number here represents the amount of power consumed by the slug/droplets from the flow in order for them to move; hence, a higher ratio $R_p = \frac{P_d}{P}$ indicates a system that is more efficient. In this case, the flow utilizes more energy into transporting the more important component in the system

(oil as the target fluid).

As shown in Fig. 6, the power number for one slug case at $T = 40^{o}C$ is 3.16×10^{-6}, which means that the slug could absorb some of the flow power and used it to move in the domain. At temperature $T = 50^{o}C$, the power number jumped to 1.85×10^{-5} and finally at $T = 60^{o}C$, the power number increased to 3.12×10^{-5}.

For the two-slugs case, the power number at $T = 40^{o}C$ is equal to zero because the slug remained stationary. For $T = 50^{o}C$, the power number jumped to 2.46×10^{-5}, indicating a better usage of the flow power. As the temperature increased to $T = 60^{o}C$, the power number increased to 4.12×10^{-5}. The power number for the droplets at $T = 20^{o}C$ is 4.42×10^{-6}, suggesting that the droplets were able to use some of the flow power in the domain. At temperature $T = 40^{o}C$ the power number jumped to 8×10^{-6} and finally at $T = 50^{o}C$ the power number increased to 1.25×10^{-5}.

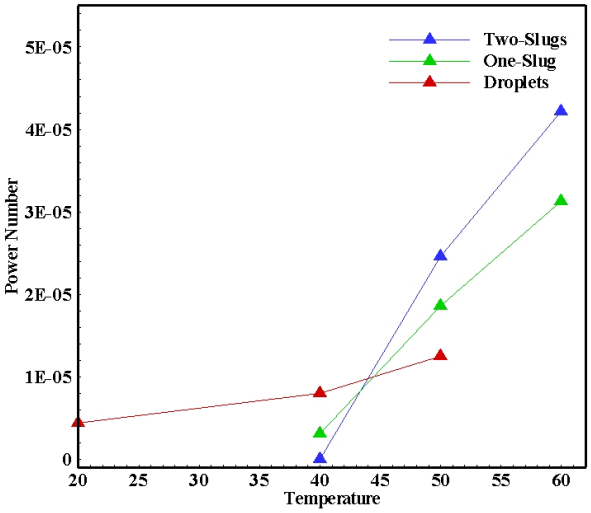

Fig. 6 Slugs and droplets power number ratios at different temperatures

From Fig. 5, it is worth noticing the power numbers curves slopes with respect to temperature. The average slope for the one slug, two slugs and droplets are $tan(\alpha_{one-slug}) = 45.56$, $tan(\alpha_{two-slug}) = 53.7$ and $tan(\alpha_{Droplet}s) = 11.88$, respectively. This stresses the fact that warming up the fluid leads to a more efficient transport system for multi slugs as compared to single slug and multi droplets.

IV. Conclusion

The model presented in this work is used to analyze the behavior of O/W systems under different thermal and surface conditions. The results for the static contact angle showed a very good agreement between the model and theoretical results at a variety of conditions. The single slug, two slugs and droplets flow simulations showed that the temperature plays an important role in controlling the velocity, power and contact angles of the system. The simulation results helped in better understanding the intricate relationship between temperature and contact angle on the mechanism for transporting O/W mixtures in confined spaces due to temperature and surface energy changes.

Acknowledgment

The authors like to thank The Higher Committee for Education Development in Iraq (HCED) for their financial support.

References

[1] Aly A. Hamouda, Omid Karoussi. Effect of Temperature, Wettability and Relative Permeability on Oil Recovery from Oil-wet Chalk. Energies 2008, 1, 19-34.
[2] Babadagli, T.; Al-Bemani, A. Investigations on matrix recovery during steam injection into heavy oil containing carbonate rocks. Journal of Petroleum Science and Engineering 2007, 58, 259-274.
[3] Babadagli, T. Temperature effect on heavy oil recovery by imbibition in fractured reservoirs. Journal of Petroleum Science and Engineering 1995, 14, 197-208.
[4] Hamouda, A. A.; Rezaei Gomari, K. A. Influence of Temperature on Wettability Alteration of Carbonate Reservoirs. Paper SPE 99848 presented at the Society of Petroleum Engineers/Department of Energy (SPE/DOE) Improved Oil Recovery Symposium, 22-26 April 2006, Tulsa, OK.
[5] Rezaei Gomari, K. A.; Karoussi, O.; Hamouda, A. A. Mechanistic Study of Interaction between Water and Carbonate Rocks for Enhancing Oil Recovery. Paper SPE 99628 presented at the Society of Petroleum Engineers (Europec/EAGE) Annual Conference and Exhibition, 12-15 June 2006, Vienna, Austria.
[6] Rezaei Gomari, K. A.; Hamouda, A. A.; Davidian, T.; Fagerland, D. A. In Contact Angle, Wettability and Adhesion; Mittal, K., Ed.; VSP: Leiden, The Netherland, 2006; Vol. 4, p.351.
[7] Rezaei Gomari, K. A.; Hamouda, A. A. Effect of Fatty Acids, Water Composition and pH on the Wettability Alteration of Calcite Surface. Journal of Petroleum Science and Engineering 2006, 50, 140-150.
[8] Rezaei Gomari, K. A.; Denoyel, R.; Hamouda, A. A. Wettability of Calcite and Mica Modified by Different Long Chain Fatty Acids (C18 Acids). Journal of Colloid and Interface Science 2006, 297, 470-479.
[9] Karoussi, O.; Hamouda, A. A. Imbibition of Sulfate and Magnesium Ions into Carbonate Rocks at Elevated Temperatures and their Influence on Wettability. Energy and Fuels 2007, 21, 2138-2146.
[10] Karoussi, O.; Hamouda, A. A. Macroscopic and nanoscale study of wettability alteration of oil-wet calcite surface in presence of magnesium and sulfate ions. Journal of Colloid and Interface Science 2008, 317, 26-34.
[11] Hamouda, A. A.; Karoussi, O.; Chukwudeme, E. A. Relative permeability as a function of temperature, initial water saturation and flooding fluid compositions for modified oil-wet chalk. In review, Journal of Petroleum Science and Engineering 2008.
[12] Al-Hadhrami, H. S.; Blunt, M. J. Thermally Induced Wettability Alteration to Improve Oil Recovery in Fractured Reservoirs. SPE Reservoir Evaluation and Engineering 2001, 4 (3), 179-186.
[13] Al-Hadhrami, H. S., Blunt, M. J., "Thermally Induced Wettability Alteration to Improve Oil Recovery in Fractured Reservoirs" Society of Petroleum Engineers, 2000.
[14] Briggs. P. J. Baron, R. P. Fulleylove R. J. and Wright, M. S., 1988. Development of heavy-oil reservoirs. J. Pet. Technol. 40(2): 1206-2 14.
[15] Bo Shi and Vijay K. Dhir, Molecular dynamics simulation of the contact angle of liquids on solid surfaces, J. Chem. Phys. 130,034705, 2009.
[16] Haibo Huang, Daniel T. Thorne, Jr., Marcel G. Schaap, Michael C. Sukop, Proposed approximation for contact angles in Shan-and-Chen-type multicomponent multiphase lattice Boltzmann.
[17] W. Hasan, H. Farhat, S. Kondaraju, Hybrid Quasi-Steady Thermal Lattice Boltzmann Model for Studying the Rheology of Surfactants Contaminated Emulsions (under review at journal of computational physics).
[18] Jagannath Venkatesan, Sangeetha Rajasekaran, Anubhav Das, Sashikumaar Ganesan, International Journal of Heat and Fluid Flow 62

(2016) 282–298.
[19] Amal Yagub, Specialized Inter-Particle Interaction LBM for Patterned Superhydrophobic Surfaces, Ph.D. dissertation, Wayne State University-2015.